

Article

Nanoscale Refractive Index Sensors Based on Fano Resonance Phenomena

Yifeng Ren ¹, Qiang Wang ^{1,2,3}, Lifang Shen ², Feng Liu ^{1,2,3}, Yang Cui ², Chuanhui Zhu ² , Zhanbo Chen ², Biyi Huang ² and Shubin Yan ^{2,*} 

¹ School of Electrical and Control Engineering, North University of China, Taiyuan 030051, China

² School of Electrical Engineering, Zhejiang University of Water Resources and Electric Power, Hangzhou 310018, China

³ Joint Laboratory of Intelligent Equipment and System for Water Conservancy and Hydropower Safety Monitoring of Zhejiang Province and Belarus, Hangzhou 310018, China

* Correspondence: yanshb@zjweu.edu.cn; Tel.: +86-186-3611-2255

Abstract: In this paper, a new refractive index sensor based on Fano resonance is introduced. It is mainly composed of two parts: a metal–insulator–metal as a base waveguide and an annular resonant cavity with a double notch and a double convex circle as a coupling structure. The sensing characteristics of the design are investigated via finite element calculations. The influence of the remaining structure parameters on the system’s sensing performance and the relationship between the wavelength corresponding to the Fano trough and the refractive index are also investigated. Furthermore, the structure is applied to refractive index sensors, resulting in a type with a sensitivity of 2740 nm/RIU and a figure of merit of 52.69.

Keywords: Fano resonance; coupling; refractive index sensing; finite element method



Citation: Ren, Y.; Wang, Q.; Shen, L.; Liu, F.; Cui, Y.; Zhu, C.; Chen, Z.; Huang, B.; Yan, S. Nanoscale Refractive Index Sensors Based on Fano Resonance Phenomena. *Photonics* **2022**, *9*, 982. <https://doi.org/10.3390/photonics9120982>

Received: 2 November 2022

Accepted: 12 December 2022

Published: 14 December 2022

Publisher’s Note: MDPI stays neutral with regard to jurisdictional claims in published maps and institutional affiliations.



Copyright: © 2022 by the authors. Licensee MDPI, Basel, Switzerland. This article is an open access article distributed under the terms and conditions of the Creative Commons Attribution (CC BY) license (<https://creativecommons.org/licenses/by/4.0/>).

1. Introduction

With the development of information technology and computer technology, higher demands are being made for the accuracy and validity of the information. Photons as information carriers have the following advantages: small interactions, a low energy loss, and a fast transmission speed [1,2]. These advantages have contributed significantly to the development of optical sensors. However, optical sensors are difficult to miniaturize and integrate into well-developed dimensions due to the limitations of the visual diffraction limit size [3,4]. Surface plasmon polaritons (SPPs), a new type of unique electromagnetic wave, are formed by the interaction of incident light with free electrons on the surface of a metal. Their outstanding advantage is that they break the diffraction limit and allow for the control of photons at sub-wavelength dimensions [5–8].

Many structures can effectively excite SPPs; among these structures, metal–insulator–metal (MIM) waveguides easily excite SPPs, so they served as the base waveguide in this study [9]. During the excitation of SPPs, the Fano resonance in optical phenomena is used as a sensing basis, taking advantage of the fact that SPPs are highly sensitive to structural morphology, geometry, and the polarization state of incident light [10–12]. A relationship between the peak Fano resonance and the refractive index of the system has been established. The Fano resonance curve is sharp and sensitive to changes in the surrounding environment, providing a new option for implementing a high-precision refractive index and related sensors [13–16]. It has already attracted extensive attention from scholars at home and abroad. Zhang et al. proposed a refractive index sensor consisting of an MIM waveguide coupled to a concentric double-ring resonant cavity with a final sensitivity (S) of 1060 nm/RIU and a figure of merit (FOM) of 203.8 [17]. Rahmatiyar et al. proposed a novel structure of a ring resonator containing circular conical defects coupled to an MIM waveguide with conical defects, where sensitivity was 1295 nm/RIU and the

figure of merit was 159.6 [18]. Chau et al. proposed an MIM waveguide coupling structure consisting of a rectangular cavity and three silver baffles with a sensitivity of 2000 nm/RIU and a figure of merit of 110 [19]. The first two structures were too insensitive, while the third was a complex composition with many parameters. The structure used in this study has few parameters and excellent sensitivity and FOM values.

A novel nano-refractive index sensor structure based on the relationship between the Fano resonance and the refractive index of the system is proposed in this study. The design uses an MIM waveguide as the base resonant cavity. It constructs a deep, resonant cavity with a double notch and a double convex circle (DNDCC) as the coupled resonant cavity, with the former as the broadband mode and the latter as the narrowband mode. The coupling excites the Fano resonance effectively. The sensing characteristics' dependence on the system's remaining parameters was further investigated, and the DNDCC structure was applied to the field of refractive index sensors [20]. The final DNDCC-type refractive index sensor achieved a sensitivity of 2740 nm/RIU and a figure of merit of 52.69.

2. Materials and Methods

Two-dimensional and three-dimensional schematics of the DNDCC structure are shown in Figure 1a,b below.

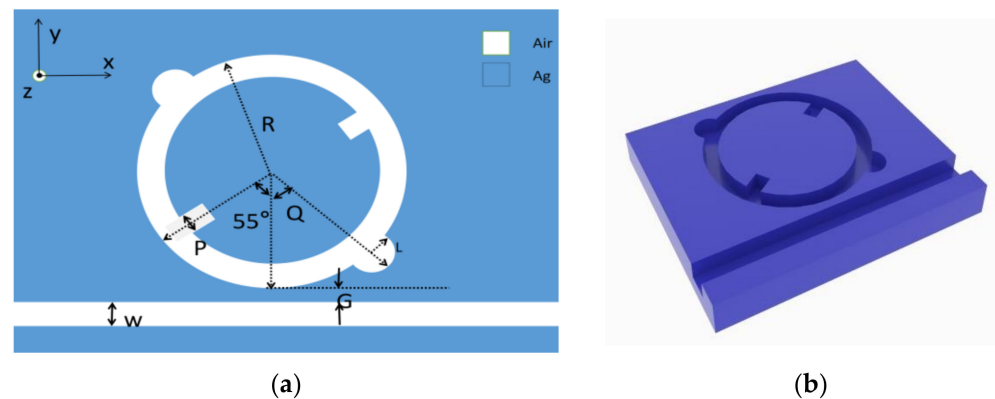


Figure 1. (a) Two-dimensional diagram of the DNDCC structure. (b) Three-dimensional diagram of the DNDCC structure.

The structure's geometrical parameters may affect the system's We defined the individual parameters in the structure, as shown in Table 1. We set a constant angle of 55° between the inner notch and the center line of the double ring. The difference in angle between the lower inner notch and the upper inner notch was set at a constant 180°. The angular difference between the lower outer convex circle and the upper outer convex circle was set at a constant 180°.

Table 1. Parameter definitions.

Name	Definition of Parameters
R	Radius of the outer ring
ω	Width of waveguide
P	Width of inner notch
G	Coupling distance between DNDCC structure and waveguide
L	Radius of the small convex ring
Q	The angle between the center line of the convex circle and the center line of the ring

SPPs propagate in the transverse magnetic mode (TM) and the transverse electric mode (TE). Only the TM mode can excite SPPs. When the ω value is small, the SPPs transmitted at the upper and lower metal–dielectric interfaces will be coupled, forming an even-symmetric and odd-symmetric dispersion model. In the odd-symmetric model, the SPPs have a short

transmission distance and a high energy loss [21,22]. The transmission distance is long in the even-symmetric model, and the energy loss is low. The even-symmetric model was used as the structure in this study. The dispersion equation for the even-symmetric model is as follows:

$$\tanh(k\omega) = \frac{-2kp\alpha_c}{k^2 + p^2\alpha_c^2} \tag{1}$$

where k is defined as the wave vector, and p is defined as the ratio of the dielectric constant (ϵ_{in}) to the metal–dielectric constant (ϵ_m). $\alpha_c = [k_0^2(\epsilon_{in} - \epsilon_m) + k]^{\frac{1}{2}}$. The equation shows that, when the incident light wave is greater than the value taken by ω , only the even-symmetric mode exists, so ω was assigned a smaller fixed value of 50 nm in this study [23,24].

The corresponding structure was created in “COMSOL Multiphysics 5.4”, and the metal Ag and air was added to the material column. The related dielectric constants were set. It is important to note that the dielectric constant of the metal varies with the frequency of the incident light and is therefore imported via the Drude model [25]. The idealized Drude model ignores the effect of electron leap and takes into account the difference between the actual and the ideal. We introduce a modified Drude model as follows [26]:

$$\epsilon(\omega) = \epsilon_\infty + \frac{\epsilon_S - \epsilon_\infty}{1 + i\omega\tau} + \frac{\sigma}{i\omega\epsilon_0} \tag{2}$$

In the equation, the relative permittivity of infinite frequency is $\epsilon_\infty = 3.8344$, the static permittivity is $\epsilon_S = -9530.5$, the relaxation time is $\tau = 7.35 \times 10^{-15}$ s, and the conductivity is $\sigma = 1.1486 \times 10^7$ s/m.

Once the material was established, we set the boundary absorption conditions to exactly match the layers used when the boundary problem was established, except for the incoming and outgoing ports [27,28]. The FEM uses a triangle as the primary cell, a DNDCC structure, and waveguide structure meshing that is predefined to hyperfine division. The rest of the meshing is predefined as conventional. Finally, we selected an appropriate working interval and calculation accuracy according to the structural changes and compared them to perform a reasonable analysis [29].

The Fano resonance waveform has different shapes for different coupling structures. The sensing parameters needed to measure the sensing characteristics of the different Fano resonance waveforms. The sensitivity and figure of merit and the sensing performance of the coupled structure are commonly used by scholars at home and abroad. The S and FOM calculation equations correspond to Equations (3) and (4):

$$S = \frac{\Delta\lambda}{\Delta n} \tag{3}$$

$$FOM = \frac{S}{FWHM} \tag{4}$$

In the above equation, $\Delta\lambda$ represents the change in wavelength corresponding to the position of the Fano trough, Δn represents the change in the refractive index, and FWHM represents the system’s bandwidth [30]. The sensitivity characterizes the amount of change in the wavelength for a unit change in the refractive index. Moreover, the FOM reflects the sharpness of the Fano resonance curve.

3. Results

Before selecting the structures for this study, we plotted the transmission curves for a single waveguide, a complete DNDCC, and a resonant ring cavity with a single notch and single convex ring (SNSCC), as shown in Figure 2 below. The red curve has a high overall transmission, is almost horizontal, and can be used as a broadband mode for the Fano resonance. The purple curve shows that the SNSCC structure has two wave troughs, and calculations show that the corresponding sensitivity of the SNSCC system at this point

is 2640 with a FOM value of 51.76. Finally, the black curve for the DNDCC shows that the number of wave troughs in this system remains the same, but D1 and D2 are shifted back to varying degrees compared to the SNSCC. The comparison of the green contours shows a slight increase in the transmittance of the D2 trough corresponding to the DNDCC compared to the SNSCC system. The final sensitivity of the DNDCC structure reaches 2740 nm/RIU, while the FOM value reaches 52.69. In summary, it can be seen that the DNDCC structure has a higher sensitivity and a better FOM value than the SNSCC, which is why we chose DNDCC as the main object of study.

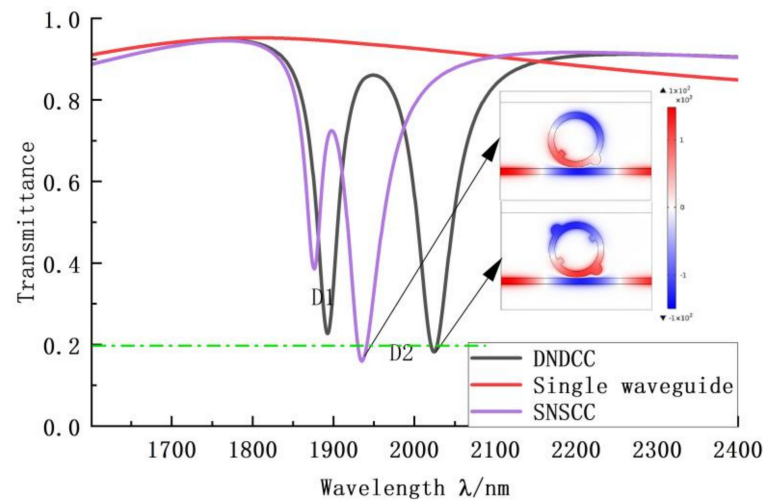


Figure 2. Transmission curve plots for DNDCC, SNSCC, and waveguide structures. Inset: Normalized magnetic field diagram for DNDCC and SNSCC structures.

The above is a comparison of the performance of the systems utilizing sensing parameters. In addition, we analyzed the normalized magnetic field graphs of the two systems. Comparing the field strength graph to the color indicator scale on the right shows that the DNDCC structure graph is darker in color, i.e., has a higher energy aggregation capability, which ultimately manifests itself in its better Fano effect and sharper curve. The ideal optical type of refractive index sensor should have a corresponding transmittance of 0.2 or less.

After selecting the DNDCC as the primary structure for study, we further explored the effect of structural parameters on the sensing performance of the system. The outer ring’s radius, R , varied to 200, 210, 220, 230, and 240 nm while the other parameters are kept constant. The graph is shown in Figure 3.

As can be seen in Figure 3a, as the radius increases, the shape of the system transmission curve remains essentially the same, and the number of transmission troughs remains the same, but the transmission curve shifts back overall. Figure 3b,c clearly show that the sensitivity of both slots D1 and D2 increases steadily as the radius increases. Finally, by analyzing the bandwidth shown in Figure 3d, it is clear that the D2 trough varies more when $R = 230$ nm and $R = 240$ nm. We then further compared the FOM values of the system. When $R = 230$ nm, the FOM value at the D2 trough is 54.89. When $R = 240$ nm, the FOM at the D2 trough is 52.69. Although the corresponding FOM value is better when $R = 230$ nm, the difference between the two FOM values is only 2.2, while the difference between the two sensitivities is as high as 266. Therefore, we set R to 240 nm.

In addition to the circle radius R , we further analyzed the dependence of the sensing performance of the system on the notch width P . Figure 4a shows that the change in notch width has a minimal effect on the D1 trough, so only D2 was analyzed for specific effects. As the width of the notch increases, the transmittance at the D2 trough increases, and the sharpness of the system’s Fano resonance curve decreases. Combined with Figure 4b, it is clear that the sensitivity of the system is also decreasing at this point. Our choice of P

should be small to achieve the desired sensing performance. In this paper, we set P to 50 nm.

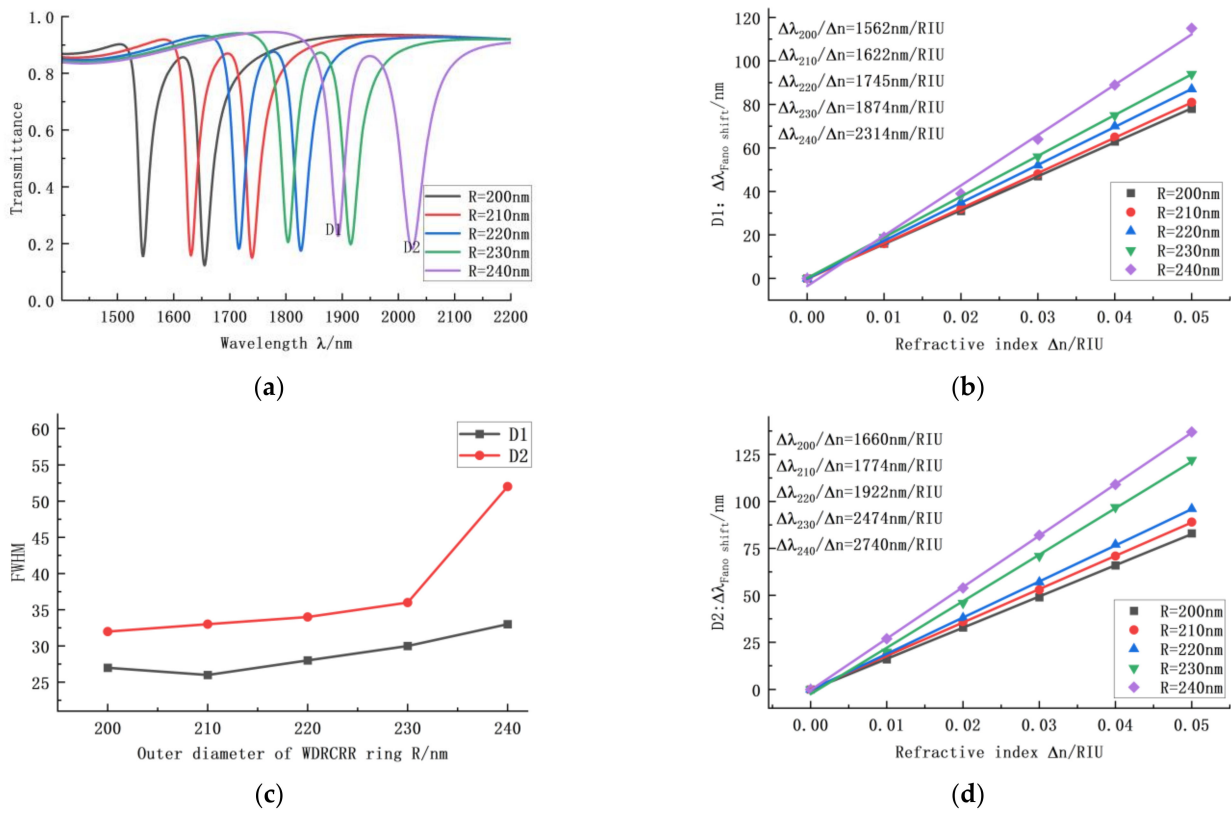


Figure 3. (a) Transmission curve spectrum when R is changed. (b) Sensitivity of the fit to the D1 trough as R changes. (c) Bandwidth plots corresponding to D1 and D2 when R is changed. (d) Sensitivity of the fit to the D2 trough as R changes.

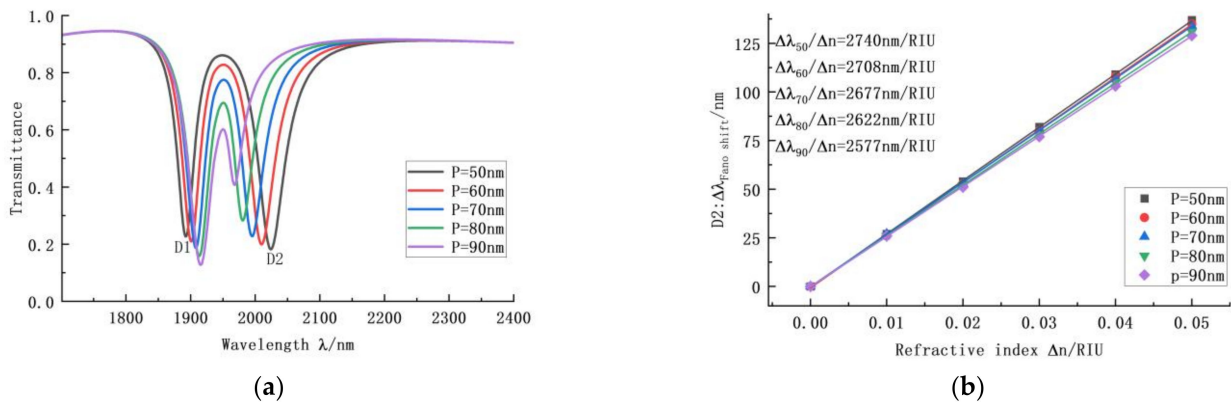


Figure 4. (a) Transmission curve spectrum when P is changed. (b) Sensitivity of the fit to the D2 trough as P changes.

Next, we further explored the effect of the radius L of the epicyclic ring on the system. The parameter L starts at 30 nm and increases in 10 nm gaps to 70 nm, while the remaining parameters are kept constant. Figure 5a shows that the transmittance is high at the D1 trough, so no further analysis was carried out. Analysis of the D2 trough indicates that, when L is less than 50 nm, the system Fano resonance effect is poor. When L is greater than 50 nm, the D2 trough position changes greatly, while its system bandwidth increases significantly. Combined with Figure 5b, it can be seen that the system’s sensitivity at the D2

trough continues to increase when L increases. Therefore, we need to determine further the optimal parameter values based on the FOM of the system. The FOM was calculated to be 47.79 when L = 60 nm and 33.26 when L = 70 nm. We settled on a moderate L—50 nm—by combining the sensitivity and FOM values.

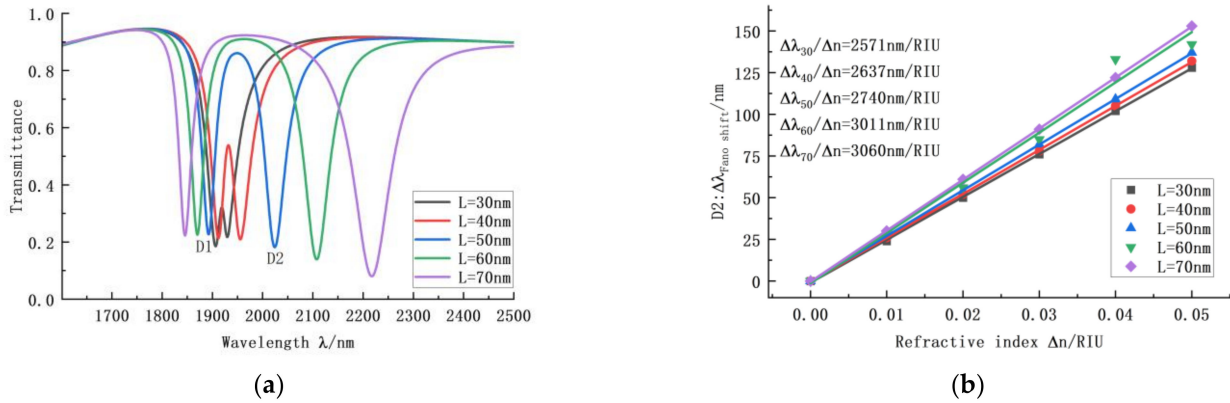


Figure 5. (a) Transmission curve spectrum when L is changed. (b) Sensitivity of the fit to the D2 trough as L changes.

The effect of the above parameters on the system is complex, and some have a pronounced effect. We can make reasonable conclusions by combining the transmission curve with the transmission requirements. As shown in Figure 6a, the transmission curve spectrum is plotted and shows that the angle Q between the convex circle and the center line is varied. As can be seen, as the angle Q increases, the D1 trough moves to the left, and the sensitivity of the system decreases, while the curve around the D2 trough becomes smoother, and the Fano resonance becomes significantly worse. Therefore, we set Q to 45°.

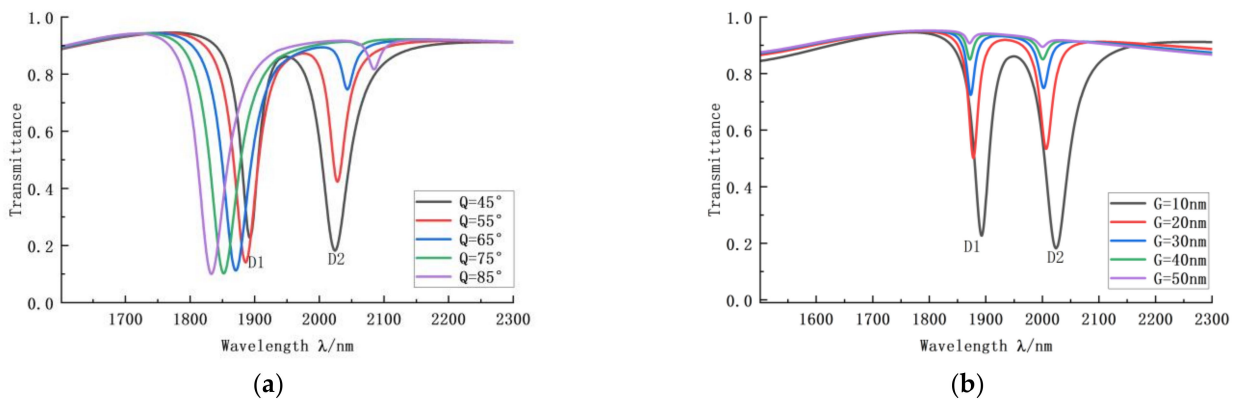


Figure 6. (a) Transmission curve spectrum when Q is changed. (b) Transmission curve spectrum when G is changed.

In addition to the influence of the structure’s parameters, the coupling distance between the waveguide and the DNDCC structure is also worth studying. Observation 6b shows that, when the coupling distance G increases, the D1 and D2 trough positions are unchanged. However, the transmission curve broadband mode increases significantly, and the narrowband mode continues to be smaller, which inevitably causes the Fano resonance effect to become worse or even eliminated. Therefore, the coupling distance G should be as small as possible. We finally set G to 10 nm.

We thus decided on the following structure parameters: R = 240 nm, P = 50 nm, L = 50 nm, G = 10 nm, and Q = 45°. After the parameters of the DNDCC structure were selected, changing the refractive index of the system led to a different degree of uniqueness in the position of the Fano trough of the transmission curve. There is always an approx-

imately linear relationship between the two. We extended this to the field of refractive index sensors.

The refractive index of the system was set in sequence from 1.00 to 1.05 in equal increments of 0.01. Figure 7a shows that, as the refractive index increases, the shape of the transmission curve of the system remains essentially constant, and the overall posterior displacement of the curve is essentially the same. Our initial guess was that the transmissivity and the valley displacement of the Fano resonance are linearly related. Combined with Figure 7b, it can be seen that the linear fit of the sensitivity of the wave valley corresponding to the D1 and D2 positions is good. Finally, with the optimal settings of all parameters, we obtained a refractive index sensor with a DNDCC structure as the main one. It has a sensitivity of 2740 nm/RIU and a figure of merit of 52.69.

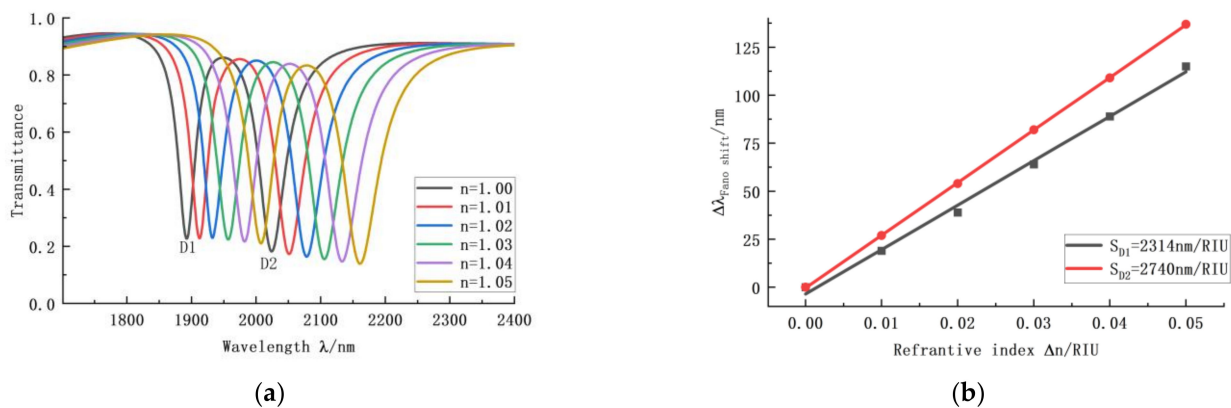


Figure 7. (a) Transmission curve spectrum for a change in refractive index n. (b) Fitted sensitivity curve of the refractive index sensor.

Finally, we showed the results of comparing the parameters of the DNDCC structure with the rest of the structures utilizing Table 2.

Table 2. Comparison of sensing parameters for different structures.

Structure	S	FOM
[17]	1060 nm/RIU	203.8
[18]	1295 nm/RIU	159.6
[19]	2000 nm/RIU	110
DNDCC	2740 nm/RIU	52.69

4. Conclusions

We have proposed a new nano-refractive index sensor consisting of an MIM waveguide as a base structure and an annular resonant cavity with a double notch and a double convex ring as a coupling structure. The system effectively excites the Fano resonance. We analyzed the influence of the parameters in the system on the sensing performance by the finite element method and selected a DNDCC structure with optimal performance. A relationship between Fano resonance and the refractive index was then established as a principle to further extend the structure used in this study to the field of refractive index sensors. The final refractive index sensor of a DNDCC structure type has a sensitivity of 2740 nm/RIU and a figure of merit of 52.69.

Author Contributions: Conceptualization, Y.R. and Q.W.; methodology, L.S.; software, Q.W. and F.L.; validation, Y.R., Q.W. and Y.C.; formal analysis, C.Z. and Z.C.; investigation, B.H.; resources, S.Y.; data curation, S.Y. and Y.R.; writing—original draft preparation, Q.W.; writing—review and editing, Y.R.; visualization, L.S. and Y.C.; supervision, C.Z.; project administration, Z.C. All authors have read and agreed to the published version of the manuscript.

Funding: This research was funded by the National Natural Science Foundation of China under Grant No. 61875250 and Grant No. 61975189, the Zhejiang Provincial Natural Science Foundation of China under Grant No. LD21F050001 and Grant No. Y21F040001, the Key Research Project by Department of Water Resources of Zhejiang Province under Grant No. RA2101, the Key Research and Development Project of Zhejiang Province under Grant No. 2021C03019, the Key R&D Projects of Shanxi Province under Grant No. 201903D421032 and 01804D131038, and the Scientific Research Foundation of Zhejiang University of Water Resources and Electric Power under Grant No. xky2022032.

Institutional Review Board Statement: Not applicable.

Informed Consent Statement: Not applicable.

Data Availability Statement: The data presented in this study are available from the corresponding author upon request.

Acknowledgments: System values are to be provided by COMSOL.

Conflicts of Interest: The authors declare that they have no conflict of interest.

References

1. Dong, B.W.; Wang, S.H.; Dong, Z.Z.; Jie, J.C.; Wang, T.M.; Li, T.J. Novel insight into dry sliding behavior of Cu-Pb-Sn in-situ composite with secondary phase in different morphology. *J. Mater. Sci. Technol.* **2020**, *40*, 158–167. [[CrossRef](#)]
2. Shi, J.; Yuan, F.; Shi, C.; Zhao, C.; Zhang, L.; Ren, L.; Zhu, Y.; Jiang, S.; Liu, Y. Statistical Evaluation of the Latest GPM-Era IMERG and GSMaP Satellite Precipitation Products in the Yellow River Source Region. *Water* **2020**, *12*, 1006. [[CrossRef](#)]
3. He, M.-D.; Liu, J.-Q.; Gong, Z.-Q.; Luo, Y.-F.; Chen, X.; Lu, W. Plasmonic splitter based on the metal-insulator-metal waveguide with periodic grooves. *Opt. Commun.* **2010**, *283*, 1784–1787. [[CrossRef](#)]
4. Jacob, J.; Babu, A.; Mathew, G.; Mathew, V. Propagation of surface plasmon polaritons in anisotropic MIM and IMI structures. *Superlattices Microstruct.* **2008**, *44*, 282–290. [[CrossRef](#)]
5. Wang, L.; Wang, L.-L.; Zeng, Y.; Xiang, D.; Zhai, X.; Li, X.; Wan, Q.; Pan, A.-I. Trapping of surface plasmon polaritons in a multiple-teeth-shaped waveguide at visible wavelengths. *Appl. Phys. A* **2010**, *103*, 883–887. [[CrossRef](#)]
6. Wang, L.; Wang, L.-L.; Zeng, Y.-P.; Xiang, D.; Zhai, X.; Li, X.-F.; Huang, W.-Q. A triangular shaped channel MIM waveguide filter. *J. Mod. Opt.* **2012**, *59*, 1686–1689. [[CrossRef](#)]
7. Yang, H.; Li, J.; Xiao, G. A highly efficient surface plasmon polaritons excitation achieved with a metal-coupled metal-insulator-metal waveguide. *AIP Adv.* **2014**, *4*, 127114. [[CrossRef](#)]
8. Zhang, Z.; Wang, H.; Zhao, Y.; Lu, D.; Zhang, Z. Transmission properties of the one-end-sealed metal-insulator-metal waveguide. *Optik* **2013**, *124*, 177–179. [[CrossRef](#)]
9. Zhu, Q.; Wang, D.; Zhang, Y. Enlargement of the band gap in the metal-insulator-metal heterowaveguide. *Opt. Commun.* **2009**, *282*, 1116–1119. [[CrossRef](#)]
10. Miroshnichenko, A.E.; Flach, S.; Kivshar, Y.S. Fano resonances in nanoscale structures. *Rev. Mod. Phys.* **2010**, *82*, 2257–2298. [[CrossRef](#)]
11. Monticone, F.; Argyropoulos, C.; Alù, A. Layered plasmonic cloaks to tailor the optical scattering at the nanoscale. *Sci. Rep.* **2012**, *2*, 912. [[CrossRef](#)] [[PubMed](#)]
12. Niu, L.; Zhang, J.B.; Fu, Y.H.; Kulkarni, S.; Lukyanchuk, B. Fano resonance in dual-disk ring plasmonic nanostructures. *Opt. Express* **2011**, *19*, 22974–22981. [[CrossRef](#)] [[PubMed](#)]
13. Sekkat, Z.; Hayashi, S.; Nesterenko, D.V.; Rahmouni, A.; Refki, S.; Ishitobi, H.; Inouye, Y.; Kawata, S. Plasmonic coupled modes in metal-dielectric multilayer structures: Fano resonance and giant field enhancement. *Opt. Express* **2016**, *24*, 20080–20088. [[CrossRef](#)] [[PubMed](#)]
14. Wang, S.; Zhao, T.; Yu, S.; Ma, W. High-Performance Nano-Sensing and Slow-Light Applications Based on Tunable Multiple Fano Resonances and EIT-Like Effects in Coupled Plasmonic Resonator System. *IEEE Access* **2020**, *8*, 40599–40611. [[CrossRef](#)]
15. Wu, T.; Liu, Y.; Yu, Z.; Peng, Y.; Shu, C.; Ye, H. The sensing characteristics of plasmonic waveguide with a ring resonator. *Opt. Express* **2014**, *22*, 7669–7677. [[CrossRef](#)]
16. Yu, S.; Zhao, T.; Yu, J.; Pan, D. Tuning Multiple Fano Resonances for On-Chip Sensors in a Plasmonic System. *Sensors* **2019**, *19*, 1559. [[CrossRef](#)]
17. Zhang, Z.; Yang, J.; He, X.; Zhang, J.; Huang, J.; Chen, D.; Han, Y. Plasmonic Refractive Index Sensor with High Figure of Merit Based on Concentric-Rings Resonator. *Sensors* **2018**, *18*, 116. [[CrossRef](#)]
18. Rahmatiyar, M.; Afsahi, M.; Danaie, M. Design of a Refractive Index Plasmonic Sensor Based on a Ring Resonator Coupled to a MIM Waveguide Containing Tapered Defects. *Plasmonics* **2020**, *15*, 2169–2176. [[CrossRef](#)]
19. Chau, Y.-F.C.; Chao, C.-T.C.; Huang, H.J.; Kooch, M.R.R.; Kumara, N.T.R.N.; Lim, C.M.; Chiang, H.-P. Ultrawide Bandgap and High Sensitivity of a Plasmonic Metal-Insulator-Metal Waveguide Filter with Cavity and Baffles. *Nanomaterials* **2020**, *10*, 2030. [[CrossRef](#)]

20. Zhu, J.; Jin, G. Detecting the temperature of ethanol based on Fano resonance spectra obtained using a metal-insulator-metal waveguide with SiO₂ branches. *Opt. Mater. Express* **2021**, *11*, 2787. [[CrossRef](#)]
21. Li, T.; Yan, S.; Liu, P.; Zhang, X.; Zhang, Y.; Shen, L.; Ren, Y.; Hua, E. A Nanoscale Structure Based on an MIM Waveguide Coupled with a Q Resonator for Monitoring Trace Element Concentration in the Human Body. *Micromachines* **2021**, *12*, 1384. [[CrossRef](#)] [[PubMed](#)]
22. Liu, P.; Yan, S.; Ren, Y.; Zhang, X.; Li, T.; Wu, X.; Shen, L.; Hua, E. A MIM Waveguide Structure of a High-Performance Refractive Index and Temperature Sensor Based on Fano Resonance. *Appl. Sci.* **2021**, *11*, 10629. [[CrossRef](#)]
23. Shi, H.; Yan, S.; Yang, X.; Su, H.; Wu, X.; Hua, E. Nanosensor Based on Fano resonance in a metal-insulator-metal waveguide structure coupled with a half-ring. *Results Phys.* **2021**, *21*, 103842. [[CrossRef](#)]
24. Yang, X.; Hua, E.; Wang, M.; Wang, Y.; Wen, F.; Yan, S. Fano Resonance in a MIM Waveguide with Two Triangle Stubs Coupled with a Split-Ring Nanocavity for Sensing Application. *Sensors* **2019**, *19*, 4972. [[CrossRef](#)] [[PubMed](#)]
25. Xu, Q.; Huang, J.; Yao, M.; Peng, S.; Zhang, J.; Peng, J.; Zhou, B.; Shen, J. Effect of S Addition on the Second Phase Particles of Zr-Sn-Nb-Fe Zirconium Alloy. *Rare Met. Mater. Eng.* **2015**, *44*, 122–125.
26. Zhang, X.; Yan, S.; Chen, Z.; Ren, Y.; Zhang, Y.; Liu, P.; Shen, L.; Li, T. Refractive index sensor based on a ring with a disk-shaped cavity for temperature detection applications. *Appl. Opt.* **2022**, *61*, 3997. [[CrossRef](#)]
27. Stocker, G.; Spettel, J.; Dao, T.D.; Tortschanoff, A.; Jannesari, R.; Pühringer, G.; Saeidi, P.; Dubois, F.; Fleury, C.; Consani, C.; et al. Ultra-Narrow SPP Generation from Ag Grating. *Sensors* **2021**, *21*, 6993. [[CrossRef](#)]
28. Yan, S.; Su, H.; Zhang, X.; Zhang, Y.; Chen, Z.; Wu, X.; Hua, E. High-sensitivity refractive index sensors based on Fano resonance in a metal-insulator-metal based arc-shaped resonator coupled with a rectangular stub. *Chin. Phys. B* **2022**, *31*, 108103. [[CrossRef](#)]
29. Kuo, C.-W.; Wang, S.-H.; Lo, S.-C.; Yong, W.-H.; Ho, Y.-L.; Delaunay, J.-J.; Tsai, W.-S.; Wei, P.-K. Sensitive Oligonucleotide Detection Using Resonant Coupling between Fano Resonance and Image Dipoles of Gold Nanoparticles. *ACS Appl. Mater. Interfaces* **2022**, *14*, 14012–14024. [[CrossRef](#)]
30. Zhao, X.; Zhang, Z.; Yan, S. Tunable Fano Resonance in Asymmetric MIM Waveguide Structure. *Sensors* **2017**, *17*, 1494. [[CrossRef](#)]